IEEE Access
Multidisciplinary | Rapid Review | Open Access Journal

Received 2 August 2023, accepted 27 August 2023, date of publication 31 August 2023, date of current version 6 September 2023.

Digital Object Identifier 10.1109/ACCESS.2023.3310542

RESEARCH ARTICLE

A Center-Fed Dual-Polarized Parallel-Plate Waveguide Slot Array Antenna Based on a Feeding Waveguide With Centered Longitudinal Feeding Slots

HUANQIAN XIONG, (Graduate Student Member, IEEE), JIRO HIROKAWA, (Fellow, IEEE), AND TAKASHI TOMURA, (Member, IEEE)

Department of Electrical and Electronic Engineering, Tokyo Institute of Technology, Tokyo 152-8552, Japan

Corresponding author: Huanqian Xiong (xiong.h.aa@m.titech.ac.jp)

ABSTRACT A dual-polarized paralle-plate waveguide slot array antenna operating at 24.5 GHz band is proposed in this paper. The radiating panel using a 5mm-thick expanded dielectric substrate ($\epsilon_r = 1.12$) consists of two orthogonally oriented 20×19 radiating slot arrays, where the slots are positioned collinearly. The centered longitudinal feeding slots are introduced into the feeding waveguides, which offer improved aperture efficiency and higher cross-polarization discrimination (XPD) compared to the conventional tilted feeding slot approach. The antenna achieves a remarkable simulated radiation efficiency of over 95% within the operation bandwidth. A prototype antenna is fabricated and verified through measurements. The measured results demonstrate an impedance bandwidth of 13%, with reflection below -10 dB. Moreover, the antenna achieves a simulated peak aperture efficiency of 54% and a measured peak antenna efficiency of 40%. The measured XPD of the antenna prototype exceeds 26 dB.

INDEX TERMS Dual-polarized antenna, parallel-plate waveguide antenna, planar array, slot antenna.

I. INTRODUCTION

Dual-polarized antennas play a crucial role in modern wireless communication systems as they offer increased channel capacity and support for full-duplex links [1]. Among various types of dual-polarized antennas, microstrip antennas have been extensively studied [2], [3], [4], [5]. While microstrip antennas can generate two orthogonal polarizations with low complexity and achieve high cross-polarization isolation, designing a large-scale antenna array requires extra effort. Existing research, such as [4], has primarily focused on enhancing the impedance bandwidth and cross-polarization discrimination (XPD) of the array elements, resulting in the fabrication of a 1×8 linear array. In microstrip array antennas, the elements are directly fed by the microstrip feeding network, necessitating two independent feeding networks for dual-polarized antennas, which may lead to higher cross-polarization levels. Additionally, the use of open transmission lines and the common edge-feed design in microstrip dual-polarized antennas can contribute to increased feeding losses.

The corporate waveguide feeding network presents a promising alternative for dual-polarized array antennas due to its lower feeding loss compared to microstrip feeding networks. Further, it offers increased design flexibility for array antennas. In the context of dual-polarized corporate-fed waveguide array antennas, a variety of dual-polarized radiating elements have been utilized, including crossed slot [6], [7], modified aperture [8], [9], [10], and ME dipole [11] designs. By designing the waveguide feeding networks on layers separate from the radiating part, the aperture size of the antenna can be used in a more efficient way. The corporate feed scheme also allows the radiating array to be divided into smaller subarrays, as a result, the design process for the dual-polarized radiating elements is simplified because of the improved isolation between

The associate editor coordinating the review of this manuscript and approving it for publication was Photos Vryonides.

elements. However, the adoption of a multi-layer structure for the corporate feeding network significantly increases the complexity of the antenna structure. Extra feeding and coupling layers are required for dual-polarization antennas, imposing limitations on the weight and increasing the cross-section of the antenna structure [6].

There is also a growing interest in developing simplified structures for single-layer dual-polarized planar slot array antennas. One approach, as presented in [12], involves integrating the feeding and radiating components into a single layer of the substrate. This design incorporates two interlaced post-wall waveguide arrays with orthogonal radiating slots. The measured antenna efficiency of the dual-polarized antenna is reduced to 22% from the theoretical value of 64% obtained with the single polarization array. This antenna effectively suppresses cross-polarization levels by introducing offset to the two arrays. Another research direction focuses on scalable single-layer dual-polarized array antennas with beam scanning characteristics, as proposed in [13] and [14]. The antenna described in [13] uses post-wall waveguides and it suffers from high dielectric losses. The edge-feed design also results in a higher transmission loss. Consequently, it achieves a modest aperture efficiency of 40% and a radiation efficiency of 76%.

Another type of linearly polarized planar array antennas typically use a single radiating layer along with feeding waveguides. These antennas commonly use either a series feed scheme or a partially corporate feed scheme [15], [16], [17]. While these schemes offer reduced design flexibility compared to antennas with a full corporate feed design, they enable the attainment of a compact structure and lower cross-section. For dual-polarized planar slot array antennas sharing similar structural characteristics, the vertical and horizontal polarizations are achieved using ridged waveguides [18], [19]. However, the complex internal structure of the radiating panels still limit their potential for large-scale production.

Parallel-plate waveguide (PPW) slot array antennas as proposed in this paper, are a type of planar waveguide antenna that utilizes a PPW for the radiating part. Its structure is further simplified by removing the walls inside the waveguide. For linearly polarized PPW slot array antennas, rectangular feeding waveguides are typically used beneath the radiating part at the center of the parallel plates [20]. However, the feeding waveguide can also be integrated into the same layer as the radiating part using post-wall waveguides, for either an edge-feed or center-feed scheme [21], [22]. Designing a linearly polarized PPW antenna poses challenges, particularly in achieving a uniform field distribution between the parallel plates. Conventional designs use feeding waveguides with tilted feeding slots, but this introduces strong transverse propagation waves that limit the aperture efficiency. To address this issue, artificial surfaces are introduced to suppress the undesired modes between the parallel plates, thus improving aperture efficiency [23]. Another method involves introducing an

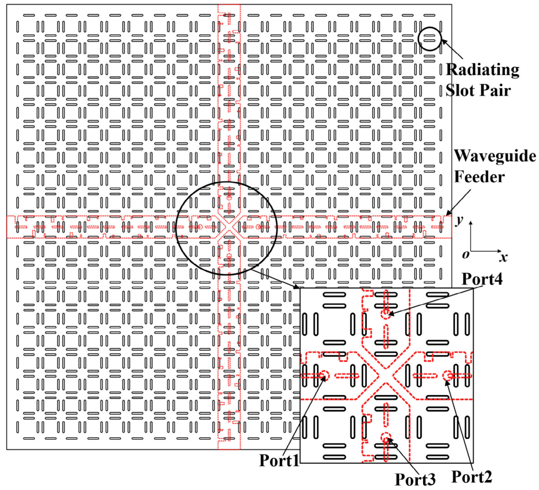

FIGURE 1. Top view of the proposed antenna.

improved feeding structure. In [24], it is demonstrated that the centered longitudinal feeding slots used in the feeding waveguides significantly increase the aperture efficiency. Designing a dual-polarized PPW slot array antenna presents further challenges due to the limited design flexibility. First, radiating slots are commonly offset to suppress mutual coupling in conventional linearly polarized PPW antennas, but this approach is not feasible for a dual-polarized antenna. Second, a single-layer structure that can accommodate feeding waveguides for two orthogonal polarizations is needed.

Here, we propose a dual-polarized PPW slot array antenna with a simple structure and low cross-section. First, we study and verify a 1×10 subarray of the collinearly positioned radiating slots, which proves suitable for the dual-polarized antenna. Second, we design a probe-fed feeding waveguide based on the centered longitudinal feeding slots proposed in [24], with a modified structure to accommodate two orthogonal feeding networks in one layer. The feeding part also features a center-feed structure, with four feeding waveguides located beneath the center of the radiating slot arrays to reduce the transmission loss. Four feeding points are also located at the center part of the antenna so a hybrid coupler can be connected directly to further reduce the transmission loss, in comparison to the edge-feed structure used in [13]. Finally, we combine four proposed feeding waveguides with a radiating panel consisting of two orthogonally positioned 20×19 radiating slot arrays. The design process and simulated results are detailed in Section III. The fabricated antenna and experimental results are illustrated in Section IV.

II. ANTENNA STRUCTURE

The proposed antenna, as depicted in Fig. 1, consists of a PPW and four waveguide feeders. It is designed to operate at a central frequency of 24.5 GHz. The PPW utilizes a 5 mm thick expanded dielectric substrate with a relative permittivity

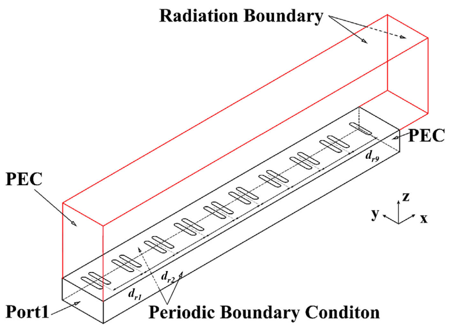

FIGURE 2. Analysis model for the subarray of radiating slots.

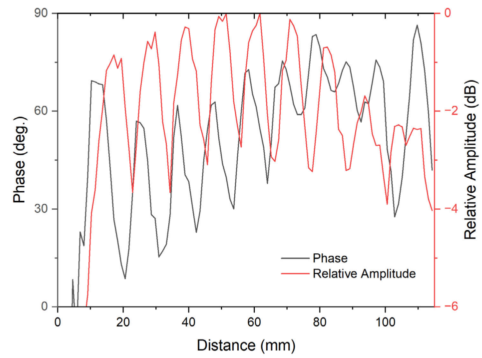

FIGURE 3. Field distributions of E_x in the x-direction.

of 1.12. Positioned beneath the PPW, two pairs of probe-fed WR-42 waveguide feeders are milled from an aluminium alloy block. Ports 1 and 2 are used for the y-polarization, and Ports 3 and 4 are used for the x-polarization.

Collinearly positioned radiating slot pairs are etched on the top plate of the PPW. The dual-polarization is realized by positioning two identical radiating slot arrays orthogonally. The waveguide feeders use centered longitudinal feeding slots to feed the PPW. Each feeding slot is paired with two inductive walls, which are used to achieve the desired coupling and suppress the reflection from the slot.

III. ANTENNA DESIGN

The radiating part and the feeding waveguide of the proposed antenna are designed separately before being combined into the full antenna.

A. SUBARRAY OF THE RADIATING SLOTS

The commonly used radiating slot pair has an offset of half the period between two slots to mitigate mutual coupling [20]. However, this structure is not suitable for the dual-polarized antenna. Fig. 2 shows the HFSS analysis model of a 1×10 subarray of the collinear radiating slot pairs. The bottom part drawn in black is the parallel plate region. A periodic boundary condition is assigned to the sidewalls to support the TEM mode and simulate the mutual coupling between subarrays. Port 1 serves as the input port for the parallel plate region, while the other end is short-ended. The elements are numbered from $k = 1$ to $k = 10$ in the x-direction. Elements $k = 1-9$ consists of a pair of radiating slots. These elements are designed to achieve a coupling of $1/(11 - k)$ and suppress the reflection. Element $k = 10$ only has a single slot to achieve 100% coupling. The red box on top represents the air box region. The end of the air box adjacent to Port 1 has a Perfect Electric Conductor (PEC) boundary, as the analysis model only includes half of the symmetrical antenna structure. The sidewalls of the air box have periodic boundaries to expand the subarray in the y-direction. The top surface and the other end are assigned with radiation boundaries.

Fig. 3 presents the phase and relative amplitude distributions of E_x in the x-direction, obtained at a distance of $\lambda_0/4$ from the radiating slot plane. Vibrations can be observed in both the relative amplitude and the phase distributions due to the spacing between the radiating slot pairs being approximately λ_g. The phase difference is smaller than 90 degrees and the lowest relative amplitude exceeds -4 dB, which illustrates proper field uniformity in the x-direction. These results verify the feasibility of using collinear radiating slot pairs in a PPW slot array antenna.

B. CENTERED LONGITUDINAL FEEDING SLOTS

To achieve coupling between the TE_{10} mode wave within the rectangular feeding waveguide and the desired TEM-like mode wave within the PPW, feeding slots are used. The conventional approach involves using tilted feeding slots, which can achieve a desired coupling by adjusting the slot angle [20]. However, research has indicated that tilted feeding slots introduce strong transverse propagating waves within the PPW. This not only limits the aperture efficiency but also increases the potential for cross-polarization in dual-polarized antennas. To get around this, we adopted the centered longitudinal feeding slots proposed in [24].

In order to design a series feeding waveguide, it is necessary to simulate the feeding slots to achieve various couplings with minimal reflection. We assign numbers to the feeding slots ranging from $n = 1$ at the center of the antenna to $n = 12$ at the edge. Three different analysis models are utilized to investigate feeding slots at different positions along the feeding waveguide.

The top and side views of the HFSS analysis model of feeding slots ($n = 3 - 11$) are shown in Fig. 4. At the bottom of the model is the rectangular feeding waveguide part, and on the top is the PPW part. Ports 1 and 2 are the input and output port of the feeding waveguide, respectively. For the top part, periodic boundaries are applied to the sidewalls to support the TEM mode wave inside the PPW and to partially simulate the mutual coupling between the feeding slots, as shown in Fig. 4a. The thickness of the slot is 0.2 mm, as shown in Fig. 4b. The required coupling of each feeding slot is defined by:

$$|S_{31}|^2 + |S_{41}|^2 = 1 - |S_{21}|^2 - |S_{11}|^2 = 1/(13 - n) \quad (1)$$

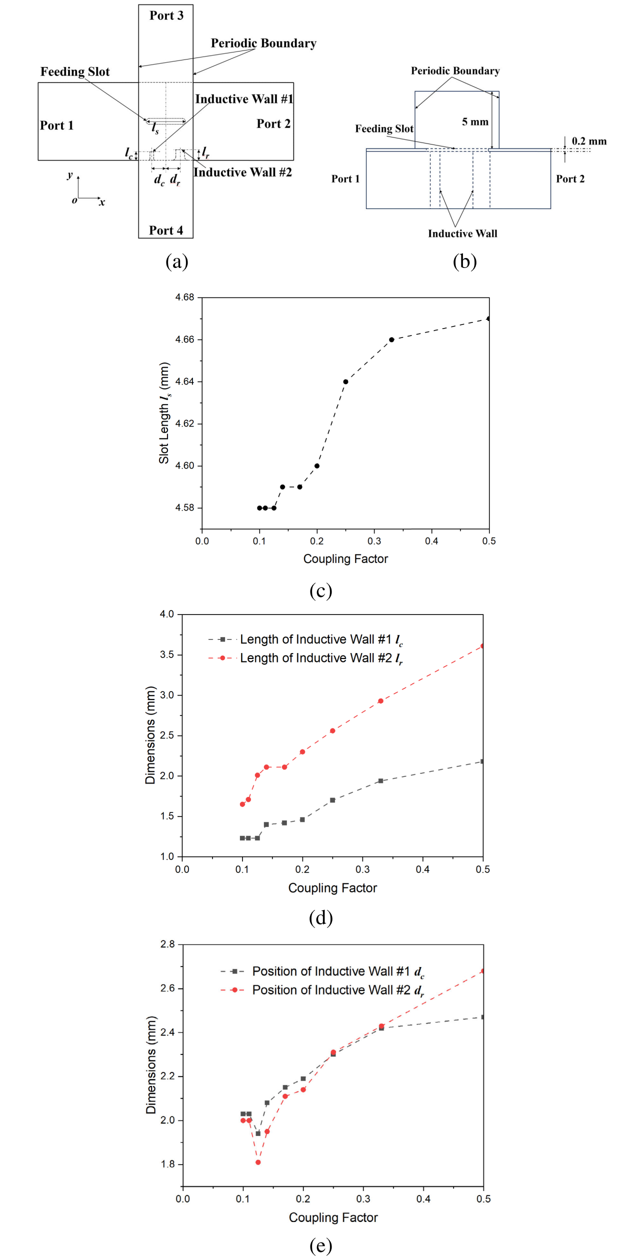

FIGURE 4. **(a) Top view of the analysis model of the feeding slot element. (b) Side view of the analysis model of the feeding slot element. (c) Slot length versus the coupling factor. (d) Wall length versus the coupling factor. (e) Wall position versus the coupling factor.**

In the design process of the slots ($n = 3-11$), the coupling is controlled by the slot length. The relationship between the slot length and the realized coupling is depicted in Fig. 4c. Other parameters related to the inductive walls shown in Fig. 4d and Fig. 4e are used to minimize the reflection from the slot. The fixed dimensions of the feeding slots are summarized in Table 1.

Fig. 5 shows the analysis model of the short-ended slot ($n = 12$). Port 1 serves as the input port of the feeding waveguide, while the other end is replaced by a PEC wall. In the previous studies on linearly polarized PPW antennas,

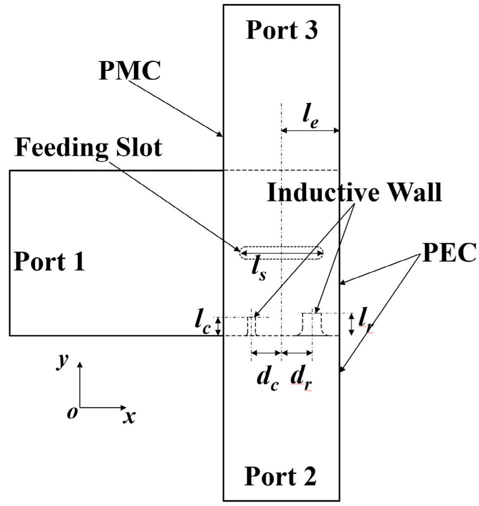

FIGURE 5. **Analysis model of the short-ended centered longitudinal feeding slot element.**

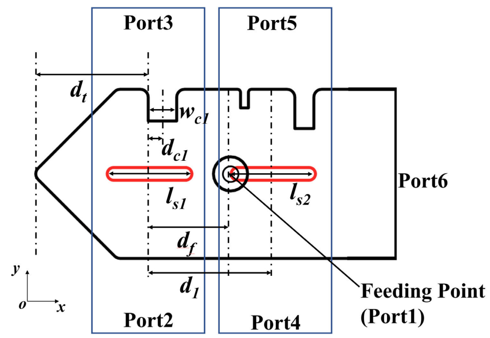

FIGURE 6. **Analysis model of the probe feeding region of the feeding waveguide.**

TABLE 1. **Fixed dimensions of the feeding slot element ($n = 3 - 11$).**

Parameters	Dimensions (mm)
Slot width w_s	0.80
Width of inductive wall #1 w_c	0.50
Width of inductive wall #2 w_r	0.80

hard walls are introduced between the parallel plates to support the desired TEM-like mode [23]. However, in the case of a dual-polarized antenna, the last radiating slot of all the radiating subarrays in two orthogonal directions is short-ended, which implies that all the sidewalls of the PPW are short-ended due to the symmetry. Additionally, on the opposite side of the parallel plate region in the short-ended element analysis model, a Perfect Magnetic Conductor (PMC) boundary is assigned instead of a periodic boundary. The slot is optimized to achieve a 100% coupling, which corresponds to minimal reflection. The design parameters of the short-ended feeding slot are detailed in Table 2.

Fig. 6 shows the analysis model of the probe feeding region of the feeding waveguide, which includes the feeding probe and the first two feeding slots ($n = 1 - 2$). In this section,

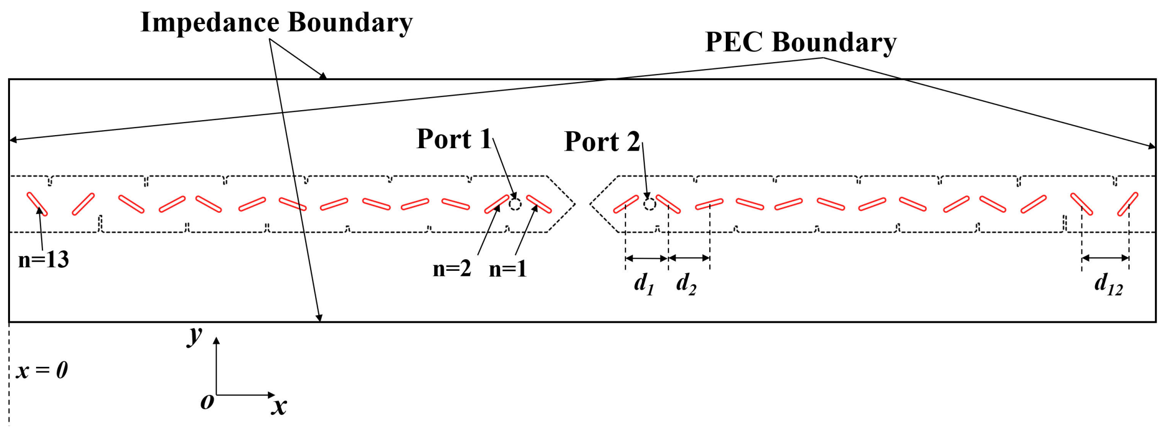

FIGURE 7. Analysis model of a pair of waveguide feeders using tilted feeding slots.

TABLE 2. Dimensions of the short-ended feeding slot element.

Parameters	Dimensions (mm)
Slot length l_s	4.96
Length of inductive wall #1 l_c	2.34
Length of inductive wall #2 l_r	3.55
Position of inductive wall #2 d_r	2.41
Position of inductive wall #2 d_r	2.23
Distance from the slot to the end l_e	5.25

TABLE 3. Dimensions of the probe feeding region of the feeding waveguide.

Parameters	Dimensions (mm)
Position of element #1 d_t	7.20
Position of the feeding point d_f	5.10
Position of element #2 d_1	7.80
Element #1	
Slot length l_{s1}	4.52
Length of inductive wall #1 l_{c1}	2.00
Width of inductive wall #1 w_{c1}	1.80
Position of inductive wall #1 d_{c1}	0.80
Element #2	
Slot length l_{s2}	4.57
Length of inductive wall #1 l_{c2}	1.21
Length of inductive wall #2 l_{r2}	1.58
Position of inductive wall #2 d_{c2}	2.02
Position of inductive wall #2 d_{r2}	1.99

only one inductive wall is utilized for the first feeding slot. Port 1 functions as the input port of the feeding probe, and Port 6 is the output port of the feeding waveguide. Ports 2 and 3 serve as the output ports of the PPW region above the feeding slot $n = 1$, while Ports 4 and 5 are the output ports of the PPW region above the feeding slot $n = 2$. To ensure that equal power is coupled through all the feeding slots, the theoretical coupling of the first two slots in this analysis model should satisfy $|S_{21}|^2 + |S_{31}|^2 = |S_{41}|^2 + |S_{51}|^2 = 0.08$ according to (1). However, an amplitude drop is observed near the center of the parallel plate region, which is also evident in the feeding waveguide using a τ-junction [24]. To enhance the uniformity of the field amplitude distribution, the coupling of the elements $n = 1$ and $n = 2$ defined above are increased to 0.14 and 0.19, respectively, in this analysis model. All the relevant dimensions are detailed in Table 3.

C. FEEDING WAVEGUIDES

To serve as a performance reference, the traditional feeding waveguides utilizing tilted feeding slots are also investigated. The HFSS analysis model of it is shown in Fig. 7. In this model, each feeding slot is tilted at a specific angle to achieve a desired coupling between the TE_{10} mode wave in the feeding waveguide and the TEM-like mode wave between the parallel plates. Since only one inductive wall is required to cancel the reflection from the tilted feeding slot, the distance d_n between the tilted feeding slots is shorter than the centered longitudinal slots, which necessitates placement of two inductive walls per feeding slot. As a result, 13 tilted feeding slots are used for each waveguide to maintain the aperture size. The HFSS analysis model of the feeding waveguides using centered longitudinal feeding slots is illustrated in Fig. 8, and there are 12 feeding slots in each waveguide.

The phase and amplitude distributions of the field between the parallel plates at 24.5 GHz are shown in Fig. 9. The reference line is positioned 19 mm (equivalent to $1.64\lambda_g$) from the center of the feeding waveguide. As may be observed in Fig. 9a, the feeding waveguides using the conventional tilted feeding slots exhibit a high level of ripples in both the amplitude and the phase distributions. The lowest relative amplitude can reach -10 dB, and the phase variations can exceed 200°. Conversely, Fig. 9b demonstrates that the utilization of the centered longitudinal feeding slots dramatically reduces the level of ripples in both amplitude and phase distributions. The lowest relative amplitude is -5 dB, and the phase variations are limited to a maximum of 120°, except that the phase climbs near the end of the waveguides due to the PEC walls. The results also show that the vibration is larger at the center part of the PPW because of the probe-feed structure. By increasing the coupling of the

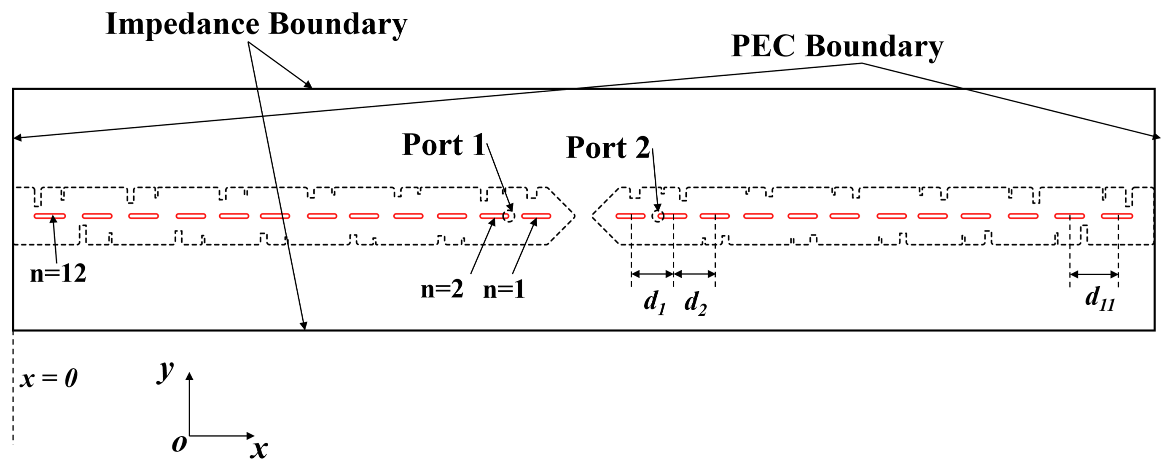

FIGURE 8. The analysis model of a pair of waveguide feeders using centered longitudinal feeding slots.

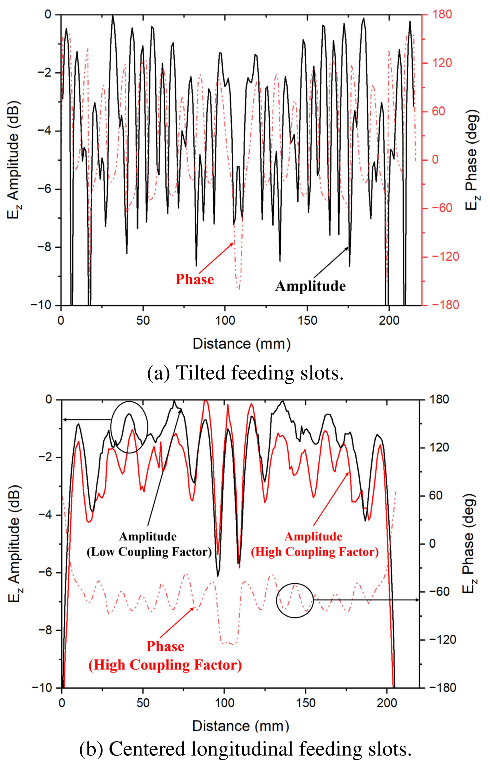

FIGURE 9. Simulated field distributions inside the PPW region at 24.5 GHz.

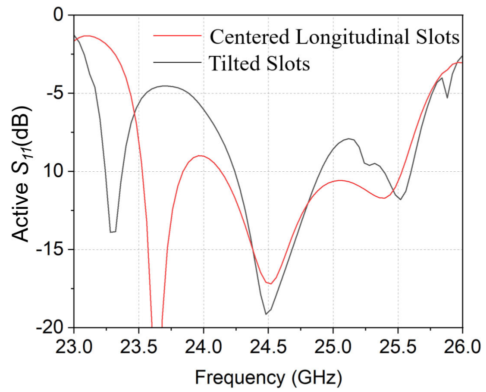

FIGURE 10. Simulated active return loss of different feeding waveguides.

first two slots, as mentioned in the previous part, we slightly enhance the uniformity of the field amplitude in the central part of the PPW. The use of the longitudinal slots also expands the working bandwidth, as shown in Fig. 10. The reflection remains below -10 dB from 24.25 GHz to 24.88 GHz for the feeding waveguide with the tilted feeding slots. For the feeding waveguide with the centered longitudinal slots, the reflection remains below -10 dB within the frequency range of 24.12 GHz to 25.55 GHz.

D. DUAL-POLARIZED PPW SLOT ARRAY ANTENNAS

Building on the two different feeding waveguide designs discussed above, the dual-polarized PPW slot array antennas are investigated here. Both antennas consist of two 20 $\times$ 19 arrays of radiating slot pairs, ensuring an equal aperture size. Fig. 11 shows the simulated radiation patterns of the two antennas. For the co-polarization component, the antenna utilizing the proposed feeding waveguide with the centered longitudinal feeding slots exhibits lower side lobe levels. Additionally, the antenna using the centered longitudinal feeding slots effectively suppresses the transverse propagation waves in the PPW region, resulting in an improved XPD of over 50 dB, compared to below 30 dB for the antenna using the conventional tilted feeding slots. Further, the peak directivity at 24.5 GHz is increased by 1.91 dB, as illustrated in Fig. 12.

IV. EXPERIMENTAL RESULTS

The proposed dual-polarized PPW slot array antenna is fabricated using a CNC milling process. Fig. 13 presents top and side views of the antenna prototype. The feeding waveguides and the frame of the PPW region are milled from

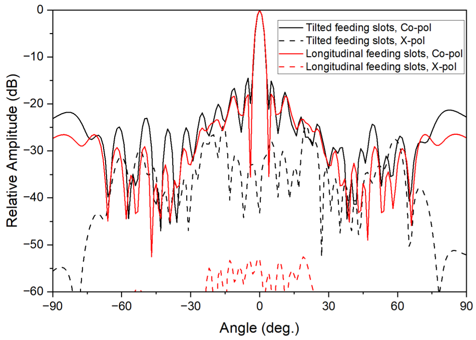

(a) E-plane radiation patterns.

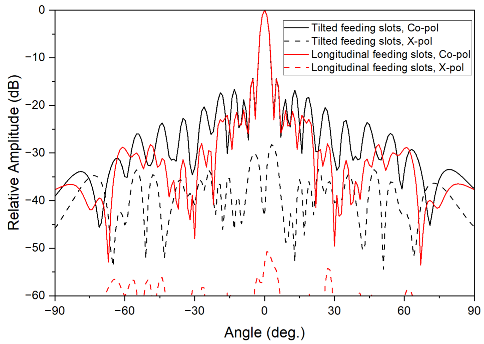

(b) H-plane radiation patterns.

FIGURE 11. **Simulated radiation patterns of antennas with different feeding waveguides.**

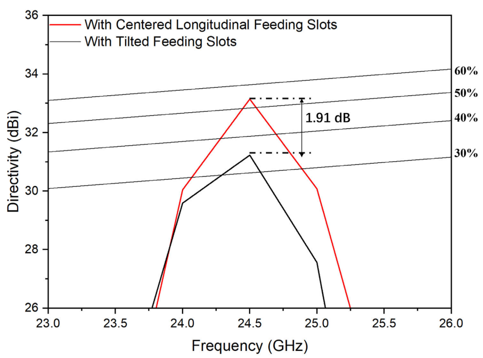

FIGURE 12. **Simulated frequency dependencies of the directivity of antennas with different feeding waveguides.**

a 5052 aluminum alloy block. The top plates of the feeding waveguides and the radiating panel are made of 0.2 mm-thick etched copper plates. The aperture size of the antenna is 213 mm × 213 mm, while the overall size of the fabricated antenna measures 245 mm × 245 mm. Four waveguide probes with a 2.92 mm-diameter connector are inserted into the feeding waveguides. To simultaneously excite two ports, a 90° hybrid coupler (Pasternack PE2CP1150) is utilized, and two coaxial cables with different lengths are introduced to compensate for the phase difference.

A. S PARAMETERS

The return losses of the antenna are measured using a vector network analyzer to obtain the active return losses.

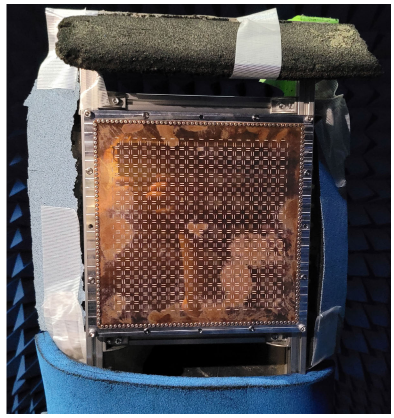

(a) Top view.

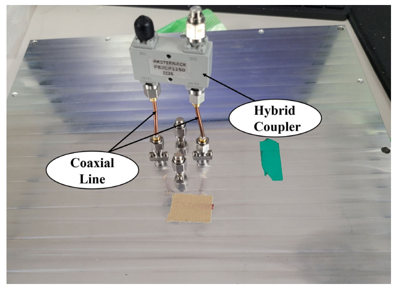

(b) Bottom view.

FIGURE 13. **The fabricated prototype antenna.**

Fig. 14 displays the measured active return losses of the antenna prototype, along with the simulated active S_{11} for reference. The measured active return loss remains below -10 dB from 23.45 GHz to 26.64 GHz for Port 1, and the measured results for the other ports also exhibit good agreement with this result. Overall, the difference between the simulated and measured results is small, only a slightly lower reflection around 26.0 GHz in the fabricated antenna. This discrepancy may be attributed to fabrication tolerances. The simulated and measured isolation between two polarizations of the antenna is shown in Fig. 15. The antenna shows good isolation, and the measured mutual coupling is below −20 dB.

B. RADIATION CHARACTERISTICS

The measured phase imbalance between the two output ports of the 90° hybrid coupler with coxial lines is smaller than 7° within the operating frequency band of the antenna. The imbalance of the insertion loss is smaller than 0.5 dB. Though the imbalance between two ports is small, the insertion loss of the hybrid coupler affects the measured antenna gain, requiring compensation using the equation: Realized gain (dB) = Measured gain (dB) - Eff_{hybrid} (dB), where the efficiency is defined as $Eff_{hybrid} = |S_{31}|^2 + |S_{41}|^2$. The measured efficiency of the hybrid coupler is shown in Fig. 16.

The measured radiation patterns for the y-polarization and the x-polarization are presented in Fig. 17 and Fig. 18. Compared to the simulated E-plane radiation patterns, the

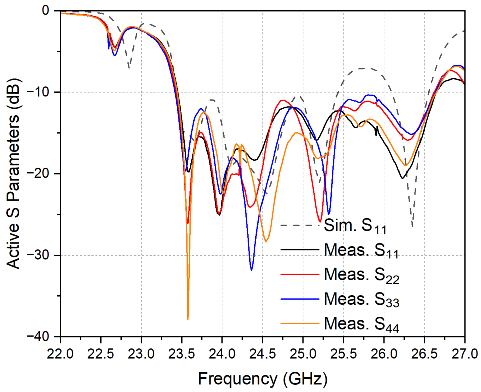

FIGURE 14. Simulated and measured active return losses.

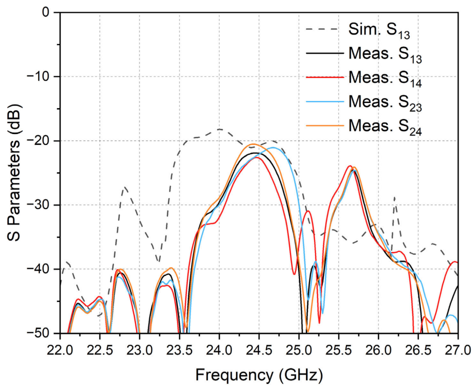

FIGURE 15. Simulated and measured isolation.

measured E-plane radiation patterns exhibit lower amplitudes of side lobes within ±60°, but with grating lobes at higher amplitudes as observed around ±75°. Regarding the H-plane radiation patterns, there is better agreement between the measured and simulated results, except for higher amplitudes of side lobes at ±5° in the measured results. These findings suggest that the radiation characteristics of the fabricated antenna agree better with the simulated results on the plane including the feeding waveguides. This phenomenon can be attributed to the feeding waveguide being less sensitive to fabrication tolerances than the PPW. Additionally, the measured XPD of the fabricated antenna exceeds 26 dB at 24.5 GHz.

Fig. 19 shows the simulated frequency dependencies of directivity and realized gain. The antenna, having an expanded dielectric substrate with the small relative permittivity of 1.12 in the PPW, achieves a high simulated radiation efficiency of above 95% from 23.0 GHz to 26.0 GHz. The measured results reveal a peak realized gain of 31.85 dBi at 24.6 GHz and a peak antenna efficiency of 40.0%. However, the measured boresight realized gain at 24.5 GHz is 1.67 dB lower than the simulated results. From the trend of the traces, it is evident that the working frequency of the fabricated antenna is higher than the simulated one, as the actual expanded dielectric substrate used has a relative

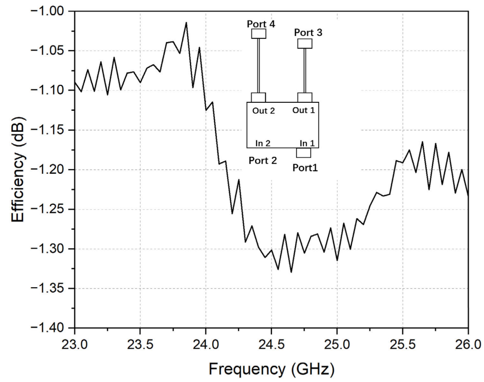

FIGURE 16. The configuration of the 90° hybrid coupler and its transmission efficiency.

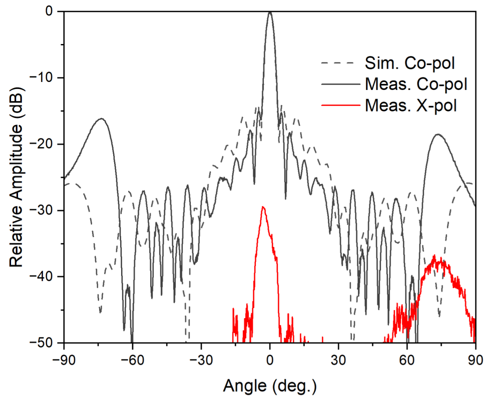

(a) E-plane radiation patterns.

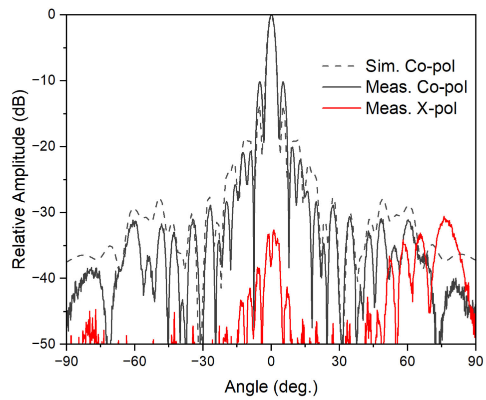

(b) H-plane radiation patterns.

FIGURE 17. Simulated and measured radiation patterns of the y-polarization.

permittivity of 1.10. Still, even when compared to the simulated results using the updated substrate parameters, the fabricated antenna still exhibits a higher working frequency, with a difference of 1.34 dBi in realized gain at 24.5 GHz.

C. ANALYSIS ON THE DIFFERENCE BETWEEN THE MEASURED AND SIMULATED RESULTS

The series-fed PPW radiating panel in the proposed antenna is sensitive to fabrication tolerances and inaccurate substrate

TABLE 4. Comparison between this work and reported dual-polarized array antennas.

Ref.	Number of Elements	Freq. (GHz)	XPD (dB)	Peak Gain (dBi)	Radiation Efficiency/ Aperture Efficiency	Antenna Structure	Feeding Type
[4]	8	1.63-2.9	25	16.0	NA/NA	Microstrip Reflector Antenna	Partially Corporate
[5]	2 × 8	26.3-28.8	25	16.7	39%/NA	Microstrip Antenna	Series
[6]	16 × 16	59-63	25	32	79%/NA	Multi-layer Laminated WG	Full Corporate
[7]	8 × 8	11.95-12.61	25	22.35	84.5%/NA	Multi-layer PPW	Partially Corporate
[9]	6 × 6	10.9-14.5	25	23	50/NA%	Cavity&Microstrip Feeding network	Full Corporate
[10]	8 × 8	130-149	45	26.4	NA/67%	Multi-layer Laminated Waveguide	Full Corporate
[13]	10 × 10	24.8-25.2	26	24.9	76%/40%	Single-layer Post-wall	Series
This work	20 × 19	23.45-26.64	26	31.85	95%/54%	PPW	Series

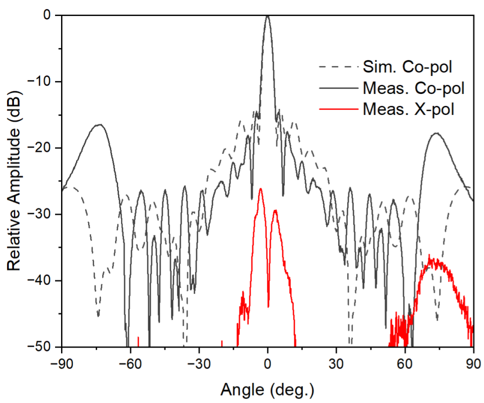

(a) E-plane radiation patterns.

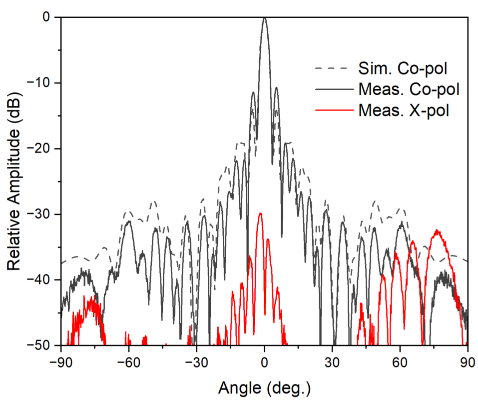

(b) H-plane radiation patterns.

FIGURE 18. Simulated and measured radiation patterns of the x-polarization.

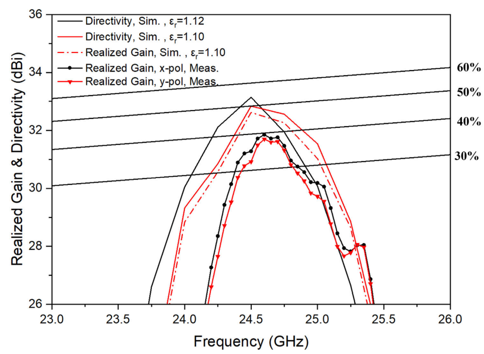

FIGURE 19. Simulated and measured boresight directivity and realized gain.

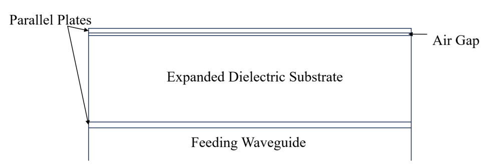

FIGURE 20. Air gap between the substrate and parallel plates.

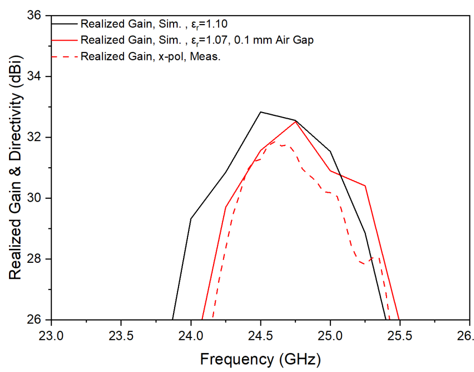

FIGURE 21. Simulated and measured realized gains with different configurations.

parameters, particularly due to the thickness of the substrate reaching 5 mm (0.43 λ_g), which is close to half of the guide wavelength.

Upon examining the fabricated antenna prototype, we observed an air gap between the substrate and the top plate of the radiating panel. This air gap arises from the weak rigidity of the thin copper plate, as suggested in Fig. 20. Through simulation analysis, we determined that even a 0.1 mm uniform air gap can significantly affect the radiating characteristics of the antenna, especially at higher frequencies. Furthermore, since the accuracy of the given relative permittivity of 1.10 may still be uncertain for the expanded dielectric substrate, we attempted to lower the permittivity to 1.07, resulting in improved agreement with the measured results, as shown in Fig. 21.

Fig. 22 illustrates why the measured boresight realized gain is significantly lower than the initial HFSS analysis model at 24.0 GHz. The main lobe of the measured E-plane

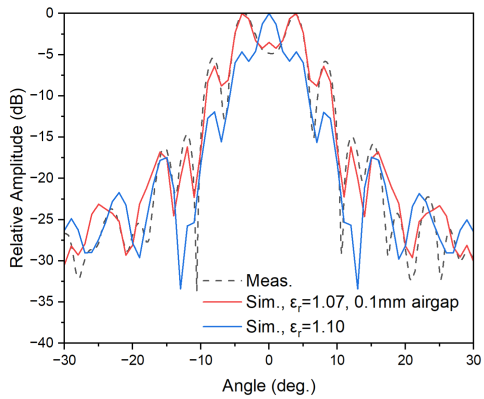

FIGURE 22. Simulated and measured E-plane radiation patterns with different configurations at 24.0 GHz (y-polarization).

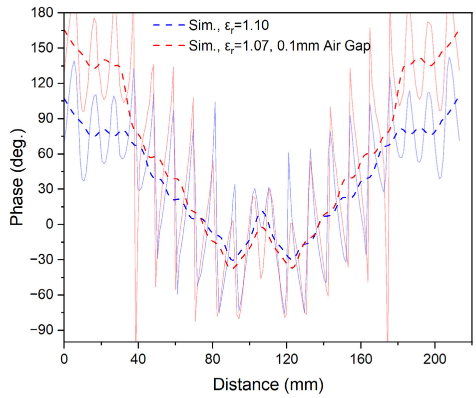

FIGURE 23. One-dimensional aperture phase distributions in the y-direction at 24.0 GHz (y-polarization).

radiation patterns is split, which can be explained by the poor uniformity in the phase distribution over the antenna aperture. By lowering the relative permittivity to 1.07 and adding the air gap in the simulation, similar radiation patterns as the measured results can be observed, as indicated by the red trace in Fig. 22. The results in Fig. 23 show how the phase distribution is influenced by the lower relative permittivity and the air gap. In summary, the assumption that the difference is caused by inaccurate substrate parameters and the air gap beneath the top plate of the radiating panel is shown to be possible.

D. PERFORMANCE COMPARISON

Table 4 summarizes the details of the antenna proposed in this paper and previously reported dual-polarized array antennas. The dual-polarized patch antenna elements used in [4] and [5] are suitable for base-station applications. However, they are typically implemented as linear arrays or with a small number of elements due to the increased complexity of the microstrip feeding network as the number of elements grows. The multi-layer laminated dual-polarized array antenna in [6] achieves good aperture efficiency but has limited impedance bandwidth. The PPW antenna proposed in [7] uses a multi-layer feeding network and can achieve higher aperture efficiency, but its impedance bandwidth is only 5.5%. The full corporate fed array antennas in [9] and [10] offer wider impedance bandwidths, but they are difficult to fabricate, and their aperture efficiency is limited. The single-layer post-wall array antenna in [13] has the smallest cross-section among the antennas listed in Table 4, but its impedance bandwidth and radiation efficiency are not ideal due to the series feed scheme and dielectric loss. The antenna proposed in this paper achieves a XPD of 26 dB in the measurement, which is only surpassed by the antenna in [10]. Although the measured antenna efficiency of the antenna proposed in this paper is reduced compared to the simulated results, it achieves a measured impedance bandwidth of 13%, and the simulated radiation efficiency exceeds 95%. Furthermore, the PPW radiating panel used in the proposed antenna can accommodate a large number of elements and is suitable for mass production due to its simplified structure.

V. CONCLUSION

A dual-polarized PPW slot array antenna operating at the 24.5 GHz band is presented in this paper. The antenna is implemented using a single-layer PPW structure and four feeding waveguides. The antenna prototype was validated with CNC milling fabrication and extensive measurements. The measured impedance bandwidth for all the four ports is 13.0%, with reflection below -10 dB. At 24.6 GHz, the measured peak realized gain reaches 31.85 dBi, accompanied by an antenna efficiency of 40%. Simulations indicate that the antenna achieves a radiation efficiency above 95% across the frequency range of 23.0 GHz-26.0 GHz, and a peak directivity of 33.14 dBi at 24.5 GHz with an aperture efficiency of 54%. To understand the disparities between the simulated and measured radiation characteristics, we performed a simulation analysis on introducing an air gap between the top plate and the substrate of the PPW. Study on the comparison between the measured results and the simulated results using various substrate parameters are also presented.

REFERENCES

[1] R. G. Vaughan, "Polarization diversity in mobile communications," *IEEE Trans. Veh. Technol.*, vol. 39, no. 3, pp. 177–186, Aug. 1990.

[2] D. M. Pozar and S. D. Targonski, "A shared-aperture dual-band dual-polarized microstrip array," *IEEE Trans. Antennas Propag.*, vol. 49, no. 2, pp. 150–157, Feb. 2001.

[3] K. L. Lau and K. M. Luk, "A wideband dual-polarized L-probe stacked patch antenna array," *IEEE Antennas Wireless Propag. Lett.*, vol. 6, pp. 529–532, 2007.

[4] Y. Cui, R. Li, and H. Fu, "A broadband dual-polarized planar antenna for 2G/3G/LTE base stations," *IEEE Trans. Antennas Propag.*, vol. 62, no. 9, pp. 4836–4840, Sep. 2014.

[5] Q. Yang, S. Gao, Q. Luo, L. Wen, Y.-L. Ban, X.-X. Yang, X. Ren, and J. Wu, "Cavity-backed slot-coupled patch antenna array with dual slant polarization for millimeter-wave base station applications," *IEEE Trans. Antennas Propag.*, vol. 69, no. 3, pp. 1404–1413, Mar. 2021.

[6] D. Kim, M. Zhang, J. Hirokawa, and M. Ando, "Design and fabrication of a dual-polarization waveguide slot array antenna with high isolation and high antenna efficiency for the 60 GHz band," *IEEE Trans. Antennas Propag.*, vol. 62, no. 6, pp. 3019–3027, Jun. 2014.

[7] X.-L. Lu, H. Zhang, S.-M. Gu, H. Liu, X.-C. Wang, and W.-Z. Lu, "A dual-polarized cross-slot antenna array on a parallel-plate waveguide with compact structure and high efficiency," *IEEE Antennas Wireless Propag. Lett.*, vol. 17, no. 1, pp. 8–11, Jan. 2018.

[8] S.-G. Zhou, G.-L. Huang, T.-H. Chio, J.-J. Yang, and G. Wei, "Design of a wideband dual-polarization full-corporate waveguide feed antenna array," *IEEE Trans. Antennas Propag.*, vol. 63, no. 11, pp. 4775–4782, Nov. 2015.

[9] S.-G. Zhou, Z.-H. Peng, G.-L. Huang, J.-Y. Li, and C.-Y.-D. Sim, "Design of wideband and dual polarized cavity antenna planar array," *IEEE Trans. Antennas Propag.*, vol. 64, no. 10, pp. 4565–4569, Oct. 2016.

[10] Y. J. Cheng, F. Y. Tan, M. M. Zhou, and Y. Fan, "Dual-polarized wideband plate array antenna with high polarization isolation and low cross polarization for D-band high-capacity wireless application," *IEEE Antennas Wireless Propag. Lett.*, vol. 19, no. 12, pp. 2023–2027, Dec. 2020.

[11] W. Zhao, X. Li, Z. Qi, and H. Zhu, "Broadband and high-gain dual-polarized antenna array with shared vias feeding network for 5G applications," *IEEE Antennas Wireless Propag. Lett.*, vol. 20, no. 12, pp. 2377–2381, Dec. 2021.

[12] S. Park, Y. Okajima, J. Hirokawa, and M. Ando, "A slotted post-wall waveguide array with interdigital structure for 45° linear and dual polarization," *IEEE Trans. Antennas Propag.*, vol. 53, no. 9, pp. 2865–2871, Sep. 2005.

[13] Q. Yang, S. Gao, Q. Luo, L. Wen, Y.-L. Ban, X. Yang, X. Ren, and J. Wu, "Dual-polarized crossed slot array antenna designed on a single laminate for millimeter-wave applications," *IEEE Trans. Antennas Propag.*, vol. 68, no. 5, pp. 4120–4125, May 2020.

[14] Y. Li, Z. Zhang, C. Deng, Z. Feng, and M. F. Iskander, "2-D planar scalable dual-polarized series-fed slot antenna array using single substrate," *IEEE Trans. Antennas Propag.*, vol. 62, no. 4, pp. 2280–2283, Apr. 2014.

[15] H. Chen, X. Hou, and L. Deng, "Design of frequency-selective surfaces radome for a planar slotted waveguide antenna," *IEEE Antennas Wireless Propag. Lett.*, vol. 8, pp. 1231–1233, 2009.

[16] P. Kumar, A. Kedar, and A. K. Singh, "Design and development of low-cost low sidelobe level slotted waveguide antenna array in X-band," *IEEE Trans. Antennas Propag.*, vol. 63, no. 11, pp. 4723–4731, Nov. 2015.

[17] M. Zhang, J. Hirokawa, and M. Ando, "An E-band partially corporate feed uniform slot array with laminated quasi double-layer waveguide and virtual PMC terminations," *IEEE Trans. Antennas Propag.*, vol. 59, no. 5, pp. 1521–1527, May 2011.

[18] T. Li, H. Meng, and W. Dou, "Design and implementation of dual-frequency dual-polarization slotted waveguide antenna array for Ka-band application," *IEEE Antennas Wireless Propag. Lett.*, vol. 13, pp. 1317–1320, 2014.

[19] M. Chen, X.-C. Fang, W. Wang, H.-T. Zhang, and G.-L. Huang, "Dual-band dual-polarized waveguide slot antenna for SAR applications," *IEEE Antennas Wireless Propag. Lett.*, vol. 19, no. 10, pp. 1719–1723, Oct. 2020.

[20] J. Hirokawa, M. Ando, and N. Goto, "Waveguide-fed parallel plate slot array antenna," *IEEE Trans. Antennas Propag.*, vol. 40, no. 2, pp. 218–223, Feb. 1992.

[21] J. Hirokawa and M. Ando, "Single-layer feed waveguide consisting of posts for plane TEM wave excitation in parallel plates," *IEEE Trans. Antennas Propag.*, vol. 46, no. 5, pp. 625–630, May 1998.

[22] K. Hashimoto, J. Hirokawa, and M. Ando, "A post-wall waveguide center-feed parallel plate slot array antenna in the millimeter-wave band," *IEEE Trans. Antennas Propag.*, vol. 58, no. 11, pp. 3532–3538, Nov. 2010.

[23] B. Pyne, P. R. Akbar, V. Ravindra, H. Saito, J. Hirokawa, and T. Fukami, "Slot-array antenna feeder network for space-borne X-band synthetic aperture radar," *IEEE Trans. Antennas Propag.*, vol. 66, no. 7, pp. 3463–3474, Jul. 2018.

[24] T. Wang, T. Tomura, J. Hirokawa, B. Pyne, P. R. Akbar, and H. Saito, "A feeding network with collinearly centered longitudinal coupling slots for a rectangular parallel-plate slot array antenna," *IEEE Trans. Antennas Propag.*, vol. 71, no. 7, pp. 5838–5849, Jul. 2023.

HUANQIAN XIONG (Graduate Student Member, IEEE) received the B.S. degree in electronic science and technology and the M.E. degree in integrated circuit engineering from Tongji University, Shanghai, China, in 2018 and 2021, respectively. He is currently pursuing the Ph.D. degree in electrical and electronic engineering with the Tokyo Institute of Technology. His research interests include millimeter wave array antenna designs, parallel plate waveguide slot array antenna designs, and applications of reinforcement learning.

JIRO HIROKAWA (Fellow, IEEE) was born in Tokyo, Japan, in 1965. He received the B.S., M.S., and D.E. degrees in electrical and electronic engineering from the Tokyo Institute of Technology (Tokyo Tech), Tokyo, in 1988, 1990, and 1994, respectively.

He was a Research Associate, from 1990 to 1996, and an Associate Professor with Tokyo Tech, from 1996 to 2015, where he is currently a Professor. He was with the Antenna Group, Chalmers University of Technology, Gothenburg, Sweden, as a Postdoctoral Fellow, from 1994 to 1995. He has authored or coauthored more than 200 peer-reviewed journal articles and more than 600 international conference presentations. His current research interests include analyses, designs, fabrication techniques of slotted waveguide array antennas, millimeter-wave, terahertz antennas, and beam-switching circuits. He is a fellow of IEICE. He served as an Associate Editor for *IEICE Transactions on Communications* (1999–2003) and (2004–2007). He also served as an Associate Editor (2013–2016) and a Track Editor (2016–2022) for IEEE Transactions on Antennas and Propagation. He has been serving as a Track Editor for IEEE Antennas and Wireless Propagation Letters, since 2023. He was the Chair of the Technical Program Committee of ISAP 2016. He was also the Chair of IEICE Technical Committee on Antennas and Propagation, from 2017 to 2019. He received the IEEE AP-S Tokyo Chapter Young Engineer Award, in 1991, Young Engineer Award from IEICE, in 1996, Tokyo Tech Award for Challenging Research, in 2003, Young Scientists' Prize from the Minister of Education, Cultures, Sports, Science and Technology in Japan, in 2005, Best Paper Award, in 2007 and the Best Letter Award, in 2009, from IEICE Communications Society, and IEICE Best Paper Award, in 2016 and 2018.

TAKASHI TOMURA (Member, IEEE) received the B.S., M.S., and D.E. degrees in electrical and electronic engineering from the Tokyo Institute of Technology, Tokyo, Japan, in 2008, 2011, and 2014, respectively. He was a Research Fellow with the Japan Society for the Promotion of Science (JSPS), in 2013. From 2014 to 2017, he was with Mitsubishi Electric Corporation, Tokyo, where he was engaged in research and development of aperture antennas for satellite communications and radar systems. From 2017 to 2019, he was a specially appointed Assistant Professor with the Tokyo Institute of Technology, where he is currently an Assistant Professor. His research interests include electromagnetic analysis, aperture antennas, and planar waveguide slot array antennas.

He is a member of the IEICE. He received the Best Student Award from Ericsson Japan, in 2012, the IEEE AP-S Tokyo Chapter Young Engineer Award, in 2015, and the Young Researcher Award from the IEICE Technical Committee on Antennas and Propagation, in 2018.